Plane-Wave Density Functional Theoretic Study of Formation of Clay-Polymer Nanocomposite Materials by Self-Catalyzed in Situ Intercalative Polymerization

Stephen Stackhouse,*,† Peter V. Coveney,*,† and Eric Sandré‡

Contribution from the Centre for Computational Science, Department of Chemistry, Queen Mary, University of London, Mile End Road, London E1 4NS, United Kingdom, and Laboratoire de Physique des Solides, Université Paris Sud, Bât. 510, 91405, Orsay, Cedex, France

Received March 13, 2001

Abstract: It has recently been shown that the intercalation and subsequent in situ polymerization of organic monomers within the interlayer of clay minerals yields nanocomposites with novel material properties. We present results of plane-wave density functional theory (DFT) based investigations into the initial stages of the polymerization of methanal and ethylenediamine within the interlayer of sodium montmorillonite. Nucleophilic attack of the amine on the aldehyde is only observed when the aldehyde is protonated or coordinated to a metal ion. No evidence is found for the dissociation of water in the hydration sphere of the sodium counterions. The Brønsted acidity of the hydroxyl groups present in the silicate layers is significantly affected by their proximity to sites of isomorphic substitution. However, the most obvious Brønsted acid sources are shown to be unlikely to catalyze the reaction. Instead catalysis is shown to occur at the clay mineral lattice-edge where hydroxyl groups and exposed aluminum ions act as strong Brønsted and Lewis acid sites, respectively.

1. Introduction

In recent years there has been considerable interest in clay−polymer nanocomposites due to the novel material qualities that they exhibit. They offer enhanced mechanical and thermal properties,[1,2] which has led to a wide range of applications in the automotive, electronics, and furnishing industries.

The intrinsic structure of clay−polymer nanocomposites varies depending on their constituents and method of preparation. Two extremes may be used to define the range of possible structures. At one extreme the intercalated polymer chains sit within the clay mineral layers, which are stacked together in a well-ordered manner. Such materials are called *intercalated* or *nonexfoliated* nanocomposites. At the other extreme the clay mineral layers have lost their order and are well dispersed in a continuous polymer matrix. Such materials are called *delaminated* or *exfoliated* nanocomposites. Some nanocomposites may, of course, contain both ordered and disordered phases. Recent research has mainly focused on the preparation of exfoliated rather than nonexfoliated materials because of their lower density.

Currently three established methods of clay−polymer nanocomposite preparation exist: exfoliation−adsorption,[3] in situ intercalative polymerization,[1,4,5] and direct polymer melt intercalation.[2,6,7] Exfoliation−adsorption involves exfoliation of the clay mineral using a solvent in which the polymer is soluble. This is followed by addition of the polymer, which is adsorbed onto the clay mineral layers. Upon evaporation of the solvent the clay mineral layers reassemble. The major disadvantage of this approach is that a suitable solvent is not always available. In situ intercalative polymerization involves mechanical mixing of the clay mineral with a monomer, which intercalates within the interlayer and promotes delamination. This is followed by polymerization of the monomer to yield linear or cross-linked polymer matrices. Polymerization may be initiated by heat or radiation, by addition of an organic initiator, or by a catalyst, such as an acid, fixed through cationic exchange inside the interlayer. However, it is often necessary to disperse the clay mineral by a preswelling step of long-chain alkylammonium ion intercalation to aid exfoliation. This is brought about by exchange of the natural interlayer cations with the organic salt. It is convenient to combine the preswelling of the clay mineral and its acid treatment. Direct polymer melt intercalation simply involves mechanical mixing of the clay mineral into a polymer melt. As with in situ intercalative polymerization, direct polymer melt intercalation usually requires some pretreatment of the clay mineral, again via exchange of the natural cations with an organic salt. However, in this case the purpose of the treatment is not to aid delamination of the clay mineral. Rather, the presence of the alkylammonium cations within the interlayer renders the hydrophilic clay mineral layers organophilic and therefore increases the enthalpic interactions with the intercalating polymer.

* Address correspondence to these authors at the following e-mail addresses: s.stackhouse@qmul.ac.uk and p.v.coveney@qmul.ac.uk.

† Queen Mary, University of London.

‡ Université Paris Sud.

(1) Kojima, Y.; Usuki, A.; Kawasumi, M.; Okada, A.; Kurauchi, T.; Kamigaito, O. *J. Polym. Sci., Part A: Polym. Chem.* **1993**, *31*, 983−986.

(2) Liu, L.; Qi, Z.; Zhu, X. *J. Appl. Polym. Sci.* **1999**, *71*, 1133−1138.

(3) Lemmon, J. P.; Wu, J.; Oriakhi, C.; Lerner, M. M. *Electrochim. Acta* **1995**, *40*, 2245−2249.

(4) Wang, M. S.; Pinnavaia, T. J. *Chem. Mater.* **1994**, *6*, 468−474.

(5) Okamoto, M.; Morita, S.; Taguchi, H.; Kim, Y. H.; Kotaka, T.; Tateyama, H. *Polymer* **2000**, *10*, 3887−3890.

(6) Vaia, R. A.; Ishii, H.; Giannelis, E. P. *Chem. Mater.* **1993**, *5*, 1694−1696.

(7) Vaia, R. A.; Jandt, K. D.; Kramer, E. J.; Giannelis, E. P. *Chem. Mater.* **1996**, *8*, 2628−2635.

10.1021/ja015808d CCC: $20.00
Published on Web 11/03/2001

A comprehensive summary of developments in the synthesis, properties, and applications of polymer-layered silicate nanocomposites is given in a recent review by Alexandre and Dubois.[8] In the present work, however, we focus on a completely new method that has recently been discovered.[9] This new synthetic route, which we shall call "self-catalyzed in situ intercalative polymerization", shares many similarities with in situ intercalative polymerization, but differs in that no pretreatment of the clay mineral or additional initiator is required and two monomers are intercalated as opposed to just one.

The purpose of the present paper is to provide theoretical insight into the mechanism of this novel synthetic process by clarifying the catalytic role played by the clay matrix. Specifically we investigate the potential of sodium montmorillonite to activate the carbonyl bond of methanal by either protonation from a Brønsted acid source or coordination to a Lewis site. We also investigate a subsequent stage by which copolymerization of methanal and ethlyenediamine may proceed. This is done by performing plane-wave DFT-based calculations on periodic models of clay systems. We believe that the work presented in this paper is the first such DFT study of an organic reaction catalyzed by a clay mineral carried out with use of a periodic model.

The paper is organized as follows. In Section 2 we discuss the work done on self-catalyzed in situ intercalative polymerization by focusing on a specific example, that of methanal reacting with ethylenediamine within the interlayer of sodium montmorillonite. Section 3 catalogues the potential sources of Brønsted and Lewis acidity in sodium montmorillonite and provides a brief discussion of the role the clay mineral architecture may play in catalysis. In Section 4 a summary is given of previous simulation studies of clay minerals, leading on to our reasoning for employing a plane-wave density functional theory (DFT) based method to study this system and a concise description of DFT itself. Section 5 provides an account of the model systems and the optimization method used, while Section 6 discusses the results of these simulations. Finally, in Section 7 we draw some conclusions from this work.

2. Self-Catalyzed in Situ Intercalative Polymerization

In recent work, Coveney et al.[9] proposed a new method of fabricating clay−polymer nanocomposites. This method involves treating a raw clay mineral (specifically sodium montmorillonite) with an aqueous solution of two monomers, which are thought to spontaneously copolymerize within the galleries of the clay. Depending on the choice of monomer combination, exfoliated or nonexfoliated materials were synthesized, both with greatly enhanced mechanical properties. Adopting a combinatorial discovery approach, Coveney et al. performed a large number of preparations using different monomer combinations. X-ray diffraction (XRD), fast-atom bombardment mass spectrometry (FAB MS), and solid-state nuclear magnetic resonance (NMR) spectroscopy were used to indicate whether any form of polymerization had occurred. These nanocomposite materials are worthy of attention since their preparation procedure requires no pretreatment of the clay mineral—the copolymerization reaction is catalyzed by the natural material—and occurs under facile conditions (aqueous environment, neutral pH, and room temperature). Potential applications exist in the furniture, construction, and petroleum industries, inter alia. However, the copolymerization mechanism operating within the clay layers is currently poorly understood; in particular it is unclear how the reactions are catalyzed by the untreated clay mineral.

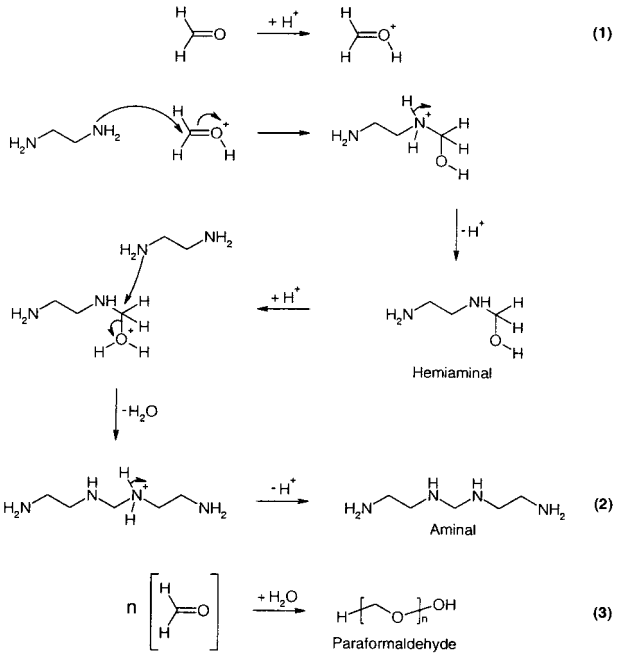

Figure 1. Proposed reaction mechanisms thought to occur within the clay interlayer: (1) protonation of methanal; (2) copolymerization of methanal with ethylenediamine; and (3) self-polymerization of methanal.

One specific pair of monomers studied by Coveney et al.[9] was methanal (CH_2O) and ethylenediamine ($NH_2CH_2CH_2NH_2$), which in addition to being cheap also formed a particularly desirable nanocomposite.

Analysis of the clay−polymer nanocomposite by XRD indicated an average clay−gallery spacing of 14.4 Å, which was unaffected by extraction with chloroform. FAB MS of the filtrate indicated evidence of polymer formation on the clay and, therefore, presumably inside also. Peaks at 90, 120, and 150 mass units were assigned to the addition of one, two, and three molecules of methanal to ethylenediamine, respectively, forming hemiaminals. Higher molecular ions at 424, 443, and 613 indicated copolymerization although they could not be assigned to definitive addition products. However, magic angle spinning ^{13}C NMR performed on an analogous Laponite nanocomposite provided evidence for the presence of hemiaminal, aminal and methylene carbon atoms, implying that copolymerization had indeed occurred.

The synthesis of Nylon 66 from hexanedioic acid and 1,6-hexanediamine is one of the most well-known examples of copolymerization.[10] The reaction is acid catalyzed and begins with the protonation of a carbonyl group of the acid, rendering it open to nucleophilic attack by a nitrogen of the amine. The addition of the amine to the acid is followed by elimination of both water and the initial acid catalyst. Methanal and ethylenediamine possess similar functional groups to those of hexanedioic acid and 1,6-hexanediamine, and it was thought that they may undergo a similar type of reaction within the interlayer of montmorillonite, as shown in Figure 1, eqs 1 and 2. Protonation of methanal is followed by nucleophilic attack by ethylenediamine leading to an initial hemiaminal addition product. Subsequent stages lead to the formation of an aminal, itself able to perform nucleophilic attack on a second methanal

(8) Alexandre, M.; Dubois, P. *Mater. Sci. Eng.: R: Rep.* **2000**, *28*, 1−63.

(9) Coveney, P. V.; Griffin, J. L. W.; Watkinson, M.; Whiting, A.; Boek, E. S. *Mol. Sim.* **2001**, in press.

(10) McMurry, J. *Organic Chemistry*, 5th ed.; Brooks/Cole Publishing: Pacific Grove, CA, 1999; p 1271.

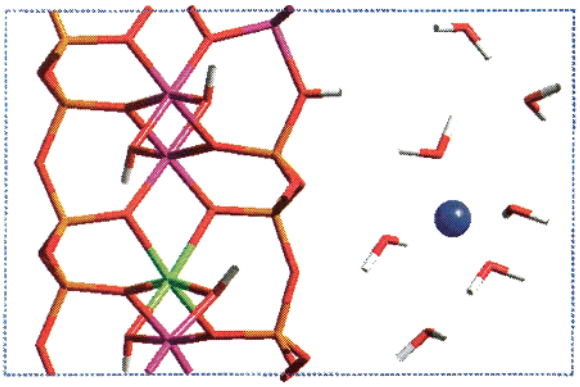

Figure 2. Sodium montmorillonite unit cell. Three-dimensional periodic boundary conditions are applied at the edges of the cell, as indicated by the blue dashed lines. The color scheme used is white for hydrogen, red for oxygen, blue for sodium, green for magnesium, pink for aluminum, and yellow for silicon.

molecule and thus generate a copolymer. In the case of the synthesis of Nylon 66, one of the monomers is an acid that auto catalyzes the reaction, albeit very slowly unless the reaction mixture is heated or an external acid source is introduced. However, neither methanal nor ethylenediamine is an acid. It is therefore reasonable to assume that the copolymerization reaction between methanal and ethylenediamine is catalyzed by sodium montmorillonite acting as a solid acid catalyst.

It is worth noting that magic angle spinning ^{13}C NMR also displayed peaks characteristic of poly-acetal carbon atoms, indicating that some self-polymerization of methanal had taken place,[9] as shown in Figure 1, eq 3. This made it difficult to conclusively assign the larger ion fragments indicated by FAB MS to a methanal−ethylenediamine copolymer since they may also be due to paraformaldehdye.

In either case, the initial stage of both reactions is likely to be the same, that is the protonation of methanal (Figure 1, eq 1) by the clay mineral. The potential of sodium montmorillonite to act as an acid catalyst is therefore of great importance in understanding the mechanism leading to the formation of these novel nanocomposites.

3. Sodium Montmorillonite as a Catalyst

Sodium montmorillonite, illustrated in Figure 2, is a 2:1 layer type aluminosilicate clay mineral comprising an octahedral alumina layer fused between two tetrahedral silica layers. Isomorphic substitution of octahedral aluminum by magnesium creates a negative structural charge, which is balanced by extraneous sodium cations adsorbed into the space between layers, called the interlayer.[11] This leads to a general formula of $[Na_xMg_xAl_{2-x}(OH)_2Si_4O_{10}]$. Hydration of the sodium ions means that it is normal for a certain amount of water to be accommodated within the interlayer where it forms hydration shells around the cations.[12]

Some isomorphic substitution of tetrahedral silicon by aluminum may also occur. In this paper we will adopt nomenclature used previously,[13] whereby montmorillonite with substitution in the octahedral layer alone is known as "Otay-type" montmorillonite and that with substitution in both the octahedral and tetrahedral layers is called "Wyoming-type" montmorillonite.

Several potential sources of Brønsted and Lewis acidity exist within the structure of sodium montmorillonite, the relative amount and strength of which depend on the degree of isomorphic substitution in the octahedral and tetrahedral layers. We will now discuss views from the literature on the nature of these putative acid sites.

3.1. Brønsted Acidity. When considering the structure of sodium montmorillonite, the most immediately obvious source of Brønsted acidity is the hydroxyl groups that bridge two aluminum atoms in the octahedral layer. These protrude into the interlayer through the hexagonal ring structure, with a diameter of approximately 6 Å, formed by the bases of six corner-sharing silicon tetrahedra.[12]

A second possible source arises when a proton attaches itself to an oxygen atom in the tetrahedral layer acting as a counterion to a negative charge created either by magnesium-for-aluminum substitution in the octahedral layer or aluminum-for-silicon substitution in the tetrahedral layer.[14] These are more accessible than the aforementioned protons.

A third potential source exists at crystal edges where the sheet structure is broken and dangling bonds are terminated by hydroxyl groups, which may act as Brønsted acid sites.[15]

However, the most important source of Brønsted acidity is widely believed to be dissociated water molecules in the hydration sphere of the interlayer exchangeable cations.[16−19] The acidity depends on the water content of the clay and, to a lesser extent, upon whether the layer charge arises mainly from substitution in the octahedral or tetrahedral layers. Acidity is maximized when the water content of the clay is low (i.e. little dissipation of M^{N+} charge by the excess water) and when highly polarizing species such as M^{3+} cations are exchanged for the naturally occurring Na^+ and Ca^{2+} ions.[18,19]

The first two sources of Brønsted acidity listed above are thought to be minor contributors to the total acidity since the hydrogens are tightly bound,[12,20] and thus the latter two sources are likely to be the most prolific. The first two sources may become more important at high temperatures or under anhydrous conditions when exchangeable cation acidity becomes very low.[12,21] (Most of the copolymerization reactions reported by Coveney et al.[9] were performed at room temperature.)

3.2. Lewis Acidity. Lewis acidity is normally associated with exposed Al^{3+} ions at broken mineral crystallite edges.[12,22] Commenting on experimental investigations by Solomon and Rosser into the polymerization of styrene by various clay minerals, Grim alleged that the greater activity shown by attapulgite, as compared with sodium montmorillonite, implies that crystal edges are involved in catalysis, since attapulgite has a much larger edge-to-surface-area ratio owing to its unusual structure.[23] Grim therefore suggested that the catalytic activity

(11) Greenwood, N. N.; Earnshaw, A. *Chemistry of the Elements*; Pergamon Press: Oxford, 1994; p 413.
(12) McCabe, R. W. *Inorganic Materials*; Bruce, D. W., O'Hare, D., Eds.; Wiley: New York, 1992; Chapter 6.
(13) Bains, A. S.; Boek, E. S.; Coveney, P. V.; Williams, S. J.; Akbar, M. V. *Mol. Sim.* **2001**, *26*, 101.
(14) Moreno, S.; Kou, R. S.; Poncelet, G. *J. Catal.* **1996**, *162*, 198−208.
(15) Vaccari, A. *Appl. Clay Sci.* **1999**, *14*, 161−198.
(16) Gregory, R.; Smith, D. J. H.; Westlake, D. J. *Clay Miner.* **1983**, *18*, 431−435.
(17) Marshall, C. L.; Nicholas, J. B.; Brand, H.; Carrado, K. A.; Winans, R. E. *J. Phys. Chem.* **1996**, *100*, 15748−15752.
(18) Nishihama, S.; Yamada, H.; Nakazawa, H. *Clay Miner.* **1997**, *32*, 645−651.
(19) Tennakoon, D. T. B.; Schlögl, R.; Rayment, T.; Klinowski, J.; Jones, W.; Thomas, J. M. *Clay Miner.* **1983**, *18*, 357−371.
(20) Trombetta, M.; Busca, G.; Lenarda, M.; Storaro, L.; Ganzerla, R.; Piovesan, L.; Lopez, A. J.; Alcantara-Rodrìguez, M.; Rodríguez-Castellón, E. *Appl. Catal.* **2000**, *193*, 55−69.
(21) Adams, J. M.; Clapp, T. V.; Clement, D. E. *Clay Miner.* **1983**, *18*, 411−421.
(22) Brady, P. V.; Cygan, R. T.; Nagy, K. L. *J. Colloid Interface Sci.* **1996**, *183*, 356−364.

was related to aluminum in octahedral coordination situated at the crystal edges.

Attenuated total reflectance Fourier transform infrared (ATR-FTIR) spectroscopy has been used to investigate the nature of chemical bonding between salicylic acid and the clay mineral illite. By correlating experimental infrared frequencies with those computed from Hartree−Fock (HF) molecular orbital calculations it was suggested that complexes form involving carboxylate oxygen atoms and Al^{3+} octahedra at the illite clay edges.[24]

3.3. Effect of Clay Mineral Architecture. The geometric structure of clay minerals is also reported to play a role in their catalytic properties. Organic species adsorbed into the clay mineral interlayer are constrained to diffuse in two-dimensional space instead of a three-dimensional volume. This increases the encounter frequencies between any reactants adsorbed into the interlayer, enhancing the reaction rate by up to 4 or 5 orders of magnitude.[25]

Experimental work by Porter et al. has shown that clay minerals adsorb, concentrate, and subsequently catalyze the polymerization of biological monomers into short peptides and oligonucleotides.[26] (We are not unaware of the relevance of our work to these applications.) Steric effects often lead to higher selectivity in reactions within clays[15] and can be enhanced by pillaring of the clay mineral.

4. Electronic Structure Modeling of Clay Minerals

In previous work we have used classical simulation methods to model the swelling of smectite clays.[13,27,28] However, such methods are unable to model the dynamics of electrons in chemical processes and are therefore not sufficient when investigating catalytic activity and chemical reactions. In cases such as this, electronic structure calculations must be performed. These may take the form of ab initio or *semiempirical* calculations.

In general, previous electronic structure studies of clay minerals have been limited by the computational requirements necessary for modeling a realistically sized clay mineral model. It has therefore been the norm to perform calculations employing localized basis sets on small, nonperiodic, cluster models considered to be representative of the bulk clay mineral. For example, Teppen et al. carried out a thorough study of a number of fragments representative of clay minerals using Hartree−Fock (HF), second-order Møller−Plesset (MP2) perturbation theory, and local DFT methods.[29] Chatterjee et al. used a DFT-based method to perform calculations on cluster models of sodium montmorillonite and were able to investigate the clay−water interface,[30] electronic and structural properties,[31] and clay−cation−water interactions.[32] The hydration of the interlayer cations has also been investigated by Gorb et al., who studied the hydration of a magnesium cation within a clay mineral using a semiempirical self-consistent-field molecular orbital linear-combination of atomic orbitals (SCF MO LCAO) method and making the minimum neglect of differential overlap Parameterized Model 3 (MNDO-PM3) approximation.[33] Marshall et al. used restricted Hartree−Fock (RHF) and MP2 methods to look at the acidity of hydrated lithium hydroxide with respect to the proton affinity of the water molecules.[18] Studies of the dissolution of clay minerals have been carried out on cluster models of clay minerals by Kubicki et al.[34] using HF calculations and Strandh et al. using a DFT-based method.[35]

These studies of cluster models provided some insight into the structural and chemical properties of clay minerals, many claiming good agreement with experimental work. The principal advantage of studying cluster models of clay minerals is that they can offer some intuitive results at a relatively modest computational cost. However, Strandh et al. conceded that the size of the model system is important,[35] while Chatterjee et al.[32] noted that it would be preferable to use a periodic clay model, since it better approximates the infinite crystal lattice and confined nature of the interlayer of clay minerals.

The method of choice for the modeling and simulation of zeolites has been DFT,[36,37] because this method, when used in conjunction with periodic boundary conditions and a plane-wave basis set, is particularly suited to the study of crystalline structures, of which zeolites and clay minerals are both examples. Indeed it is the only modeling method capable of simulating systems large enough to provide a realistic representation of a zeolite structure, while also allowing one to follow the dynamics of electrons in chemical processes, necessary when studying catalysis.

Density functional theory, based on the Hohenberg−Kohn theorem,[38] provides a valuable alternative to more traditional quantum chemical calculations such as HF. It is still in principle an ab initio technique since it is based on a parameter-free theory. The problem it attempts to solve is identical to that of the HF method, in that it tries to find the lowest energy geometry of a system of interacting electrons moving in an electric field generated by an arrangement of the fixed nuclei, by reducing the task to that of solving a set of one-electron wave function equations known as the Kohn−Sham equations.[39] However, it treats the electron−electron interaction differently from conventional ab initio methods, making use of a *local density approximation* or *generalized gradient approximation* to derive an approximate expression for the exchange and correlation operators. This results in a substantial reduction in calculation time and thus DFT methods can be applied to larger systems, with existing computational resources.

When studying periodic systems using a DFT-based method a natural choice for electron density representation is a plane-wave basis set. Bloch's theorem states that, in a periodic solid, each electronic wave function can be described as the product of a cell-periodic part and a plane-wave-like part.[40] The cell-periodic part of the wave function can be expressed by using a

(23) Grim, R. E. *Clay Mineralogy*; McGraw-Hill Book Company: New York, 1968; pp 388−392.
(24) Kubicki, J. D.; Itoh, M. J.; Schroeter, L. M.; Apitz, S. E. *Environ. Sci. Technol.* **1997**, *31*, 1151−1156.
(25) Cheng, S. *Catal. Today* **1999**, *49*, 303−312.
(26) Porter, T. L.; Eastman, M. P.; Whitehorse, R.; Bain, E.; Manygoats, K. *Scanning* **2000**, *22*, 1−5.
(27) DeSiqueira, A. V. C.; Skipper, N. T.; Coveney, P. V.; Boek, E. S. *Mol. Phys.* **1997**, *92*, 1−6.
(28) Boek, E. S.; Coveney, P. V.; Skipper, N. T. *J. Am. Chem. Soc.* **1995**, *117*, 12608−12617.
(29) Teppen, B. J.; Yu, C−H.; Newton, S. Q.; Miller, D. M.; Schäfer, L. *J. Mol. Struct.* **1998**, *445*, 65−88.
(30) Chatterjee, A.; Iwasaki, T.; Ebina, T.; Hayashi, H. *Appl. Surf. Sci.* **1997**, *121*, 167−170.
(31) Chatterjee, A.; Iwasaki, T.; Hayashi, H.; Ebina, T.; Torii, K. *J. Mol. Catal. A: Chem.* **1998**, *136*, 195−202.
(32) Chatterjee, A.; Iwasaki, T.; Ebina, T.; Miyamoto, A. *Comput. Mater. Sci.* **1999**, *14*, 119−124.
(33) Gorb, L. G.; Aksenenko, E. V.; Adams, J. W.; Larson, S. W.; Weiss, C. A.; Leszczynska, D.; Leszczynski, J. *J. Mol. Struct.* **1998**, *425*, 129−135.
(34) Kubicki, J. D.; Blake, G. A.; Apitz, S. E. *Geochim. Cosmochim. Acta* **1997**, *61*, 1031−1046.
(35) Strandh, H.; Pettersson, L. G. M.; Sjöberg, L.; Wahlgren, U. *Geochim. Cosmochim. Acta* **1997**, *61*, 2577−2587.
(36) Štich, I.; Gale, J. D.; Terakura, K.; Payne, M. C. *J. Am. Chem. Soc.* **1999**, *121*, 3292−3302.
(37) Sandré, E.; Payne, M. C.; Gale, J. D. *Chem. Commun.* **1998**, *22*, 2445−2446.
(38) Hohenberg, P.; Kohn, W. *Phys. Rev. B* **1964**, *136*, 864−871.
(39) Kohn, W.; Sham, L. J. *Phys. Rev. A* **1965**, *140*, 1133−1138.

basis set consisting of a discrete set of plane-waves whose wave vectors are reciprocal lattice vectors of the crystal. Therefore each electronic wave function can be written as a sum of plane-waves. **k**-point sampling is used to select a certain set of reciprocal space vectors (**k**-points) at which each wave function should be calculated, with the size of the set governed by the accuracy required.

To efficiently implement a plane-wave basis set it is also necessary to make the pseudopotential approximation, which replaces the core electrons and strong nuclear potential with a weaker pseudopotential. This reduces the number of plane-waves necessary to represent the electronic wave functions by removing the highly oscillatory wave functions of the electrons in the core region. A comprehensive description of DFT and its use in conjunction with periodic boundary conditions, a plane-wave basis set, norm-conserving pseudopotentials, and **k**-point sampling is given by Payne et al.[41]

Considering the similarity between the chemical structure and behavior of clay minerals and zeolites, it is reasonable to expect that plane-wave DFT methods should be well suited to the study of catalysis in clay minerals. Indeed, the method has already been applied in one study of clay mineral systems. Bridgeman et al. used a DFT method employing a plane-wave basis set and pseudopotentials to study periodic models of talc and pyrophyllite and their interaction with water.[42] Studying periodic models of clay minerals is computationally very expensive, but as noted earlier, such calculations are more accurate since they model the infinite crystal lattice and also the nature of the clay interlayer. Other ab initio methods have also been used to study a clay mineral employing periodic boundary conditions in three dimensions, for example, Hess and Saunders studied kaolinite using HF LCAO calculations.[43]

5. Simulation Details

In this section we describe the optimization method used, development of the model systems, and investigation into the interaction of the monomers with the various acid sites. We also give some technical details concerning these calculations.

5.1. Optimization Method. Calculations based on plane-wave density functional theory were performed with the CASTEP code,[41] which utilizes periodic boundary conditions, a plane-wave basis set, and **k**-point sampling. This was an updated version of the code used by Bridgeman et al. to study the structure of talc and pyrophyllite and their interactions with water.[42] Ultrasoft pseudopotentials were employed.[44] The energy cutoff for the plane wave expansion was 340 eV and just one special **k**-point was allowed in the Brillouin zone, situated at (0.25, 0.00, 0.00). For all simulations the form of the exchange−correlation functional used adhered to the generalized gradient approximation (GGA).[45,46]

5.2. Model Systems. Since montmorillonites are naturally disordered in the planes of the clay layers very little structural data is available in the common international X-ray crystallographic databases, where only the unit cell parameters are found.[47] However, a periodic model of potassium muscovite (disregarding hydrogen atomic positions) is obtainable from a structural database.[48] The structures of the aluminosilicate layers of muscovite and montmorillonite differ only in the type of isomorphic substitution that they exhibit. Muscovite is characterized by substitution of silicon by aluminum in the tetrahedral layer and montmorillonite by substitution of aluminum by magnesium in the octahedral layer,[11] as well as, in some cases, a small amount of tetrahedral substitution. Initially a periodic unit cell of pyrophyllite was produced from the muscovite model. Pyrophyllite has identical aluminosilicate layers to both muscovite and montmorillonite, but exhibits no isomorphic substitution in either the tetrahedral or octahedral layer.[11] The pyrophyllite model of unit cell formula $[Al_2(OH)_2Si_4O_{10}]_2$ was assigned the unit cell parameters calculated from crystallographic data for montmorillonite[47] and optimized with no atom or cell constraints imposed. (By "optimized" we mean that the total energy of the cell was minimized.)

The optimized pyrophyllite unit cell was used as a template for the fabrication of three Otay-type and six Wyoming-type montmorillonite systems, each characterizing a different arrangement of isomorphic substitution. The Otay-type montmorillonite systems were ascribed one substitution of aluminum by magnesium in the octahedral layer, which was balanced by a proton counterion attached to one of the oxygen atoms in the tetrahedral layer. This gave each system a unit cell formula of $[MgAl_3(OH)_4(Si_4O_{10})_2H]$. The Wyoming-type montmorillonite systems were developed from the Otay-type models by further substitution of one silicon by aluminum in the tetrahedral layer. To avoid possible overcrowding in the interlayer and to keep the systems simple no additional counterion was introduced to balance the extra isomorphic substitution. This gave each model a unit cell formula of $[MgAl_3(OH)_4(AlSi_7O_{20})H]^-$.

The crystallographic database[47] listed a very small montmorillonite unit cell *c* parameter of 9.07 Å, which corresponds to a low interlayer separation. (The unit cell *c* parameter regulates the magnitude of the interlayer separation.) The low value is typical of a dehydrated clay sample; at this value no organic molecules could be accommodated between the clay layers. Since we intended to explore the potential of the Brønsted acid sites within the interlayer to protonate methanal and ethylenediamine, it was necessary to calculate a new unit cell *c* parameter corresponding to a *d*-spacing large enough to accommodate the monomers.

Preliminary investigations showed that for our clay−monomer model systems, the initial alignment of a monomer with respect to the hydroxyl group located in the tetrahedral layer affected the potential for protonation of the monomers during optimization. Protonation was found to be induced to the greatest extent in the following situations: (i) the angle between the oxygen atom in the tetrahedral layer, the proton, and the acceptor atom of the monomer was approximately 180°; (ii) in the case of methanal, the angle between the proton, the oxygen acceptor atom, and the carbon atom was approximately 120°; and (iii) in the case of ethylenediamine, the angles between the proton, the nitrogen acceptor atom, and the other atoms bonded to the nitrogen were approximately 109°. The total energy of the clay−monomer systems was also lowest when such geometries were adopted. These observations are easily explained in terms of hydrogen bonding and the preferred geometry of the protonated species and indicate that protonation is most likely when the interlayer separation is large enough to allow the monomers to align as prescribed above. Further investigations involving the optimization of relevant clay−monomer model systems over a range of interlayer separations showed that a *d*-spacing corresponding to a unit cell *c* parameter of approximately 13 Å was appropriate. The various montmorillonite model systems were consequently assigned a unit cell *c* parameter of 13 Å and optimized with no atom or cell constraints imposed.

Periodic models of montmorillonite that exhibited a lattice-edge were developed from the pyrophyllite and montmorillonite models. This was achieved by breaking all bonds that crossed the periodic plane created by the **b** and **c** lattice vectors. Oxygen atoms were then terminated with a hydrogen atom and non-oxygen atoms with a hydroxyl group, except for the exposed aluminum atom in the octahedral layer. The

(40) Ashcroft, N. W.; Mermin, N. D. *Solid State Physics*; Harcourt College Publishers: Orlando, 1976; p 133.
(41) Payne, M. C.; Teter, M. P.; Allan, D. C.; Arias, T. A.; Joannopoulos, J. D. *Rev. Mod. Phys.* **1992**, *64*, 1045−1097.
(42) Bridgeman, C. H.; Buckingham, A. D.; Skipper, N. T.; Payne, M. C. *Mol. Phys.* **1996**, *89*, 879−888.
(43) Hess, A. C.; Saunders, V. R. *J. Phys. Chem.* **1992**, *96*, 4367−4374.
(44) Vanderbilt, D. *Phys. Rev. B* **1990**, *41*, 7892−7895.
(45) Perdew, J. P.; Chevary, J. A.; Vosko, S. H.; Jackson, K. A.; Pederson, M. R.; Singh, D.; Fiolhais, C. *Phys. Rev. B* **1992**, *46*, 6671−6687.
(46) White, J. A.; Bird, D. M. *Phys. Rev. B* **1994**, *50*, 4954−4957.
(47) Wyckoff, R. W. G. *Crystal Structures*; John Wiley and Sons: Chichester, 1968; Vol. 4, p 372.
(48) *Cerius*^{2} *4.2*; Molecular Simulations Inc.: 9685 Scranton Road, San Diego, CA 92121-3752.

exposed aluminum atom was instead coordinated with two water molecules, as is observed for the clay mineral attapulgite, which occurs naturally with exposed metal ions in the octahedral layer due to its unusual structure.[49] To accommodate the extra atoms it was necessary to increase the unit cell *b* parameter. These models were then optimized with all cell parameters and central octahedral metal ions fixed.

5.3. Interaction of Monomers with Acid Sites. During the polymerization reaction an unknown mixture of sodium ions, water molecules, protons, methanal, and ethylenediamine may be present within the interlayer driving the clay layers apart. However, because of the complexity of the potential energy surface that would result from trying to model each of these species and the small size of the system cell, it was decided to model only those interactions between the clay mineral surface and the monomers. The absence of water is justified to a certain extent by the fact that organic molecules, driven by entropic factors, are usually absorbed into the interlayer with the expulsion of water.[13]

Molecular models of both methanal and ethylenediamine molecules were constructed and their geometries optimized by using semiempirical methods: specifically, the Austin Model 1 (AM1) for methanal and modified intermediate neglect of differential overlap 3 (MINDO3) for ethylenediamine on the basis of literature recommendations.[50] These were then introduced into the periodic clay unit cells and positioned manually. To explore the interaction of the monomers with the Brønsted acid sites of the clay, the monomers were positioned so as to induce protonation, i.e. as close as possible to their expected lowest energy geometry, described above. In the case of the Lewis acid sites the monomers were simply coordinated to the metal atoms. In this manner model systems were created with each monomer interacting with all of the various types of acid site. These models were optimized with all cell parameters fixed, necessary because of the absence of water and/or any additional monomers holding the clay layers apart. The positions of the octahedral metal ions were also fixed during optimization to reduce calculation times, a constraint expected to have negligible impact on the system since the energy required to cause distortion in the aluminosilicate layers is extremely large. Similar approximations were previously made by Hess et al. in their work on kaolinite.[43]

Model systems designed to investigate non-clay−mineral−surface interactions, i.e. those between methanal, ethylenediamine, water, and sodium ions, were created with no representation of the clay mineral. These models were fabricated by the desired species being manually positioned in an adequately sized, empty periodic box and optimized with all cell parameters fixed.

5.4. Computational Details. The smaller calculations were run serially on a Silicon Graphics Octane workstation mounted with two 225 MHz MIPS R10000 processors and 1GB RAM. The larger calculations were run in parallel on a Silicon Graphics Onyx2 mounted with sixteen 400 MHz MIPS R12000 processors and 8GB RAM. The code scaled well for our simulations. For example, geometry optimization of a montmorillonite unit cell containing a single methanal molecule experienced a speed-up of 1.68, 3.70, 7.30, and 13.33 when using 2, 4, 8, and 16 processors, respectively. (Here "speed-up" is defined as the ratio of the time required for the single-CPU execution to the time required for execution on *N* processors.)

6. Results and Discussion

In this section we present the main results from our simulations and discuss their implications. We begin with the in vacuo studies of interactions between methanal and ethylenediamine, and cation hydration. This is followed by a description of the optimized clay mineral structures and the interaction of methanal and ethylenediamine with their various acid sites.

6.1. Reaction of Methanal with Ethylenediamine. The nucleophilic attack of ethylenediamine upon methanal was investigated by performing simulations in vacuo, as described in Section 5.3. These showed that nucleophilic attack of ethylenediamine on methanal only occurs when methanal is activated either by protonation or coordination to a sodium cation, with increased carbonyl bond lengths of 1.2479 and 1.2175 Å, observed in these cases, respectively, compared to the in vacuo value of 1.2090 Å. The length of the nitrogen−carbon bond formed between the monomers was 1.5401 and 1.5917 Å for the proton and sodium cation activated cases, respectively. Even though coordination to a sodium cation is able to activate methanal toward nucleophilic attack from ethylenediamine it does so to a much lesser extent than by protonation. Moreover, it is thought that under anhydrous conditions the sodium cation would attach to the negatively charged interlayer surface, which would inhibit coordination of methanal. Hydration of the sodium counterion would also inhibit coordination of methanal. In either case then, coordination of methanal to a sodium cation is thought to be unlikely.

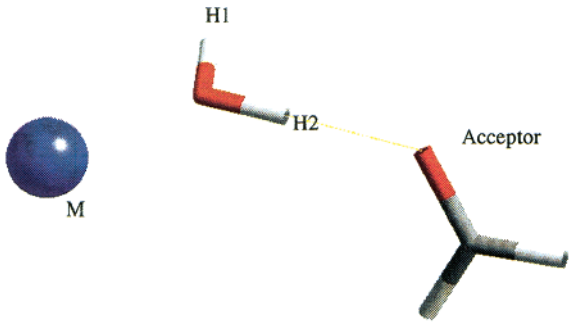

Figure 3. Example of a cation−water-monomer model system. The sodium cation is hydrated by one water molecule, which is aligned to procure protonation of methanal. The dashed yellow line indicates a hydrogen bond. The color scheme here is white for hydrogen, gray for carbon, blue for sodium, and red for oxygen. The labels define bonds referred to in Table 1.

6.2. Brønsted Acidity of Dissociated Water. Investigations into dissociation of water were also performed in vacuo. Three model systems were built for each cation studied, each comprising the metal cation hydrated by one water molecule, which was aligned so as to protonate a second water molecule, a methanal molecule, or an ethylenediamine molecule. Although these represent extreme approximations to the actual environment found within the interlayer of a clay mineral, such studies are very informative. Density functional calculations on cluster models carried out by Chatterjee et al. indicate that five water molecules hydrate sodium cations in montmorillonite.[32] However, work by Marshall et al.[17] on the hydration of lithium hydroxide showed that the highest acidity for a $Li(H_2O)_n$ complex arises when $n = 1$. These authors found that acidity is controlled by the effective charge on the cation; stabilization of this charge by coordinated water molecules causes a reduced acidity at higher hydration coordination numbers. Since under experimental circumstances this number could vary depending on conditions within a smectite clay, examination of the extreme case of just one coordinated water molecule should show if protonation by this mechanism is at all possible.

Figure 3 illustrates an example of a cation−water−monomer system; in this case the cation is sodium and the monomer methanal. Table 1 lists bond lengths of the optimized cation−water−monomer systems: M−O is the bond between the metal cation and the oxygen of the water molecule and O−H1 and O−H2 are the two hydroxyl bonds of the water molecule, where H2 is the hydrogen directed toward the acceptor atom. (Note that where dissociation of the water molecule occurred only one hydroxyl bond length is reported.) One can see that a sodium

(49) Barrer R. M. *Zeolites and Clay Minerals as Sorbents and Molecular Sieves*; Academic Press: London, 1978; p 416.

(50) Lipkowitz, K. B.; Boyd, D. B. *Reviews in Computational Chemistry*; VCH Publishers: New York, 1990; Chapter 2.

Table 1. Selected Bond Lengths of Optimized Cation−Water-Monomer Models (Å)[a]

metal cation	acceptor atom	M−O	O−H1	O−H2
Na^+	**O**H_2	2.1517	0.9703	1.0028
Na^+	**N**$H_2(CH_2)NH_2$	2.1418	0.9709	1.0491
Na^+	**O**CH_2	2.1516	0.0713	1.0045
Mg^{2+}	**O**H_2	1.8194	0.9753	
Mg^{2+}	**N**$H_2(CH_2)NH_2$	1.8164	0.9745	
Mg^{2+}	**O**CH_2	1.8251	0.9740	
Al^{3+}	**O**H_2	1.5731	0.9923	
Al^{3+}	**N**$H_2(CH_2)NH_2$	1.6410	0.9822	
Al^{3+}	**O**CH_2	1.5877	0.9902	

[a] No value indicates a dissociated bond.

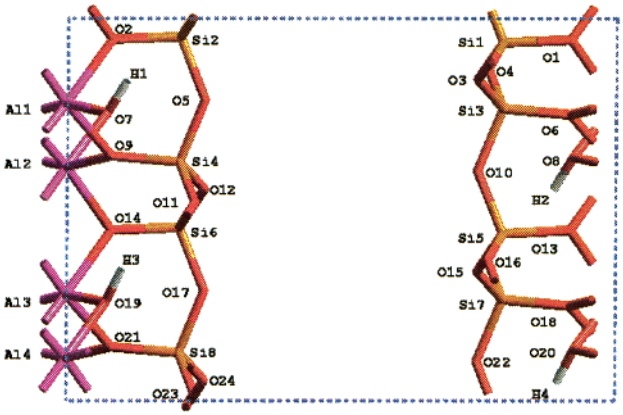

Figure 4. Optimized pyrophyllite unit cell. Three-dimensional periodic boundary conditions are applied at the edges of the cell, as indicated by the blue dashed lines. The color scheme is the same as that used in Figure 2. The atoms are labeled according to their element type and number.

Table 2. Optimized Montmorillonite Unit Cells

clay model system	octahedral substitution	tetrahedral substitution	location of proton counterion
Otay-Type 1	Al3 → Mg		O17
Otay-Type 2	Al3 → Mg		O12
Otay-Type 3	Al3 → Mg		O5
Wyoming-Type 1	Al3 → Mg	Si6 → Al	O17
Wyoming-Type 2	Al3 → Mg	Si6 → Al	O12
Wyoming-Type 3	Al3 → Mg	Si6 → Al	O5
Wyoming-Type 4	Al3 → Mg	Si2 → Al	O17
Wyoming-Type 5	Al3 → Mg	Si2 → Al	O12
Wyoming-Type 6	Al3 → Mg	Si2 → Al	O5

cation is unable to polarize a water molecule sufficiently to cause it to dissociate, while both the magnesium and aluminum cations are, resulting in the protonation of the monomers. The expected effect of increasing charge density of the cation can be observed in the M−O and O−H1 bond lengths, which are shortened and lengthened, respectively.

6.3. Clay Mineral Structure. In this subsection the optimized clay−mineral unit cells are described. Special attention is given to the Brønsted acid sites, specifically the hydroxyl groups present.

6.3.1. Montmorillonite Unit Cell. Figure 4 shows the optimized pyrophyllite unit cell, looking directly onto the *bc* plane. The isomorphic substitution displayed by the nine montmorillonite unit cells constructed is described in Table 2, making reference to the atom labels in Figure 4. They are characterized by the substitution that they exhibit in their octahedral and tetrahedral layers and the location of the hydroxyl group in the tetrahedral layer (indicated by reference to the oxygen atom). The Otay-type unit cells show the hydroxyl group in the tetrahedral layer at an increasing distance from the

Table 3. Unit Cell Parameters of Optimized Clay Mineral Models[a]

unit cell parameter	*a*	*b*	*c*	α	*β*	*γ*
experiment	5.18	8.96	9.97	90.0	99.9	90.0
pyrophyllite	5.15	8.93	13.17	90.5	99.2	89.7
Otay-Type 1	5.18	9.02	13.24	90.3	99.0	89.7
Otay-Type 2	5.19	9.02	13.46	90.2	98.6	89.7
Otay-Type 3	5.19	9.02	13.30	90.4	98.7	89.7
Wyoming-Type 1	5.23	9.07	13.79	90.2	98.8	89.8
Wyoming-Type 2	5.21	9.16	13.68	90.2	98.0	89.6
Wyoming-Type 3	5.23	9.10	13.72	90.4	98.8	89.6
Wyoming-Type 4	5.22	9.13	13.50	90.3	98.7	89.7
Wyoming-Type 5	5.24	9.10	13.55	90.2	98.3	89.8
Wyoming-Type 6	5.23	9.07	13.56	90.2	98.7	89.7

[a] Lengths are given in Å and angles in deg.

Table 4. O−H Bond Lengths of Optimized Clay Mineral Models (Å)

bond[a]	O7−H1	O8−H2	O19−H3	O20−H4	ON−H5[b]
Pyrophyllite	0.9692	0.9696	0.9698	0.9694	
Otay-Type 1	0.9739	0.9702	0.9720	0.9667	0.9799
Otay-Type 2	0.9753	0.9700	0.9719	0.9678	0.9792
Otay-Type 3	0.9750	0.9702	0.9716	0.9670	0.9788
Wyoming-Type 1	0.9723	0.9738	0.9710	0.9692	0.9729
Wyoming-Type 2	0.9736	0.9725	0.9701	0.9693	0.9732
Wyoming-Type 3	0.9727	0.9733	0.9700	0.9688	0.9743
Wyoming-Type 4	0.9726	0.9670	0.9705	0.9690	0.9753
Wyoming-Type 5	0.9746	0.9707	0.9692	0.9701	0.9769
Wyoming-Type 6	0.9737	0.9720	0.9676	0.9702	0.9701

[a] O−H bond labels refer to Figure 4. [b] For N refer to "location of proton counterion" in Table 2.

Table 5. *ab*−O−H Angles of Optimized Clay Mineral Models (deg)

bond[a]	O7−H1	O8−H2	O19−H3	O20−H4	ON−H5[b]
pyrophyllite	+28.5900	−28.8526	+22.4123	−24.8278	
Otay-Type 1	+2.2359	−27.3418	−0.5492	−19.8069	+72.0708
Otay-Type 2	+5.0196	−27.8606	−7.9510	−12.1117	+89.1664
Otay-Type 3	+1.7588	−26.4700	+1.8369	−20.2794	+84.6272
Wyoming-Type 1	+5.7709	−7.6525	+6.6290	−2.5330	+37.7159
Wyoming-Type 2	+8.9667	−14.7356	+3.8364	−5.0846	+84.5190
Wyoming-Type 3	+5.4776	−8.4345	+26.9881	−4.8715	+84.3239
Wyoming-Type 4	+15.6502	−15.4476	−0.8420	−6.1526	+54.0220
Wyoming-Type 5	+18.5998	−17.3097	−4.0414	−1.7403	+78.3519
Wyoming-Type 6	+8.6314	−11.2606	−32.9866	−3.1879	+74.7146

[a] O−H bond labels refer to Figure 4. [b] For N refer to "location of proton counterion" in Table 2.

magnesium-for-aluminum substitution in the octahedral layer. The Wyoming-type unit cells model the same arrangements of magnesium-for-aluminum substitution and hydroxyl group as the Otay-type unit cells, but with aluminum-for-silicon substitution in the tetrahedral layer, in the first instance close to and in the second instance away from the magnesium-for-aluminum substitution in the octahedral layer.

The unit cell parameters of the optimized clay mineral models are listed in Table 3. Those reported from crystallographic data for montmorillonite[47] are also listed for comparison. Of the clay mineral unit cells optimized, ones with parameters most similar to those reported experimentally for montmorillonite are clearly those of pyrophyllite and the Otay-type montmorillonites. This is as expected, confirming that the degree of substitution in montmorillonite is low and is mainly magnesium-for-aluminum in the octahedral layer. In general there is good agreement between the sets of parameters. Comparison of atomic positions was not possible since no corresponding experimental data could be found.

Tables 4 and 5 respectively list the bond length of each hydroxyl group and the angle it makes with the *ab* plane in the optimized clay mineral models. The hydroxyl bond lengths give an indication of Brønsted acidity, while the orientation of the

hydroxyl bonds give an indication of its accessibility to potential acceptor molecules. Our results show that both bond lengths and angles are affected by local isomorphic substitution; hydroxyl groups located in the octahedral and tetrahedral layers show very different behavior, but within like layers similar behavior is observed.

The bond length of the hydroxyl groups in the octahedral layer is larger for those further from magnesium in the octahedral layer and nearer to aluminum in the tetrahedral layer. Conversely, the bond length of the hydroxyl groups in the tetrahedral layer is larger for those nearer to magnesium in the octahedral layer and further from aluminum in the tetrahedral layer. However, since the observed differences are less than one-hundredth of an angstrom all hydroxyl groups in the same layer can be considered to have effectively equal Brønsted acidity. Comparison of the octahedral hydroxyl bond lengths for pyrophyllite with those calculated by a similar plane-wave DFT method shows excellent agreement, Bridgeman et al.[42] reporting 0.97 Å. In contrast, an ab initio RHF calculation on a cluster model[29] reported comparatively shorter hydroxyl bond lengths, the largest values of 0.963 and 0.962 Å being for a HF/3-21G* method.

The orientation of the octahedral hydroxyl bonds with respect to the *ab* plane is similar for each clay mineral type studied. In pyrophyllite, characterized by no substitution, all octahedral hydroxyl groups tend to make a moderate angle of on average ±25.9890° with the *ab* plane. In the Otay-type montmorillonite, characterized by substitution in the octahedral layer, octahedral hydroxyl groups on one side of the silicate layer tended to make a moderate angle of on average −22.3126° with the *ab* plane, while those on the other side made an very small angle of on average +0.3918°. In the Wyoming-type montmorillonite, characterized by substitution in both the octahedral and tetrahedral layers, octahedral hydroxyl groups tend to make a small angle of, on average, ±13.1573° with the *ab* plane. The hydroxyl bonds located in the tetrahedral layer follow a more general trend, being much smaller closer to the site of octahedral substitution. The position of these hydrogen atoms is of interest since they are not easily deduced by experiment. Comparisons with previous plane-wave DFT calculations on pyrophyllite mentioned above are reasonable, with Bridgeman et al.[42] reporting +22.23° as the angle made by the octahedral hydroxyl groups with the *ab* plane. Periodic ab initio Hartree−Fock calculations of the clay mineral kaolinite performed by Hess and Saunders indicated its analogous octahedral hydroxyl groups make an angle of +3.1° with the *ab* plane.[43]

6.3.2. Montmorillonite Lattice-Edge Unit Cell. Periodic models of montmorillonite, which possessed an exposed crystallite edge, were developed from the optimized pyrophyllite and Otay-type 1 montmorillonite models. Figure 5 shows the optimized pyrophyllite lattice-edge model. The distance between neighboring images, i.e. between the top edge of the silicate layer and the periodic cell (as pictured), is ∼6.0 Å, which we assume to be sufficiently large to be able to ignore interactions between periodic images. The unit cell parameters of the lattice-edge models were fixed during optimization and so were identical with those of the models from which they were constructed, apart from *b*, which was increased to 17.5 Å to accommodate the terminating hydroxyl groups and water molecules.

The oxygen−hydrogen bond lengths of the hydroxyl groups are listed for the two optimized lattice-edge models in Table 7, Appendix A. If we compare the bond lengths of the octahedral hydroxyl groups of the lattice-edge models with their analogues

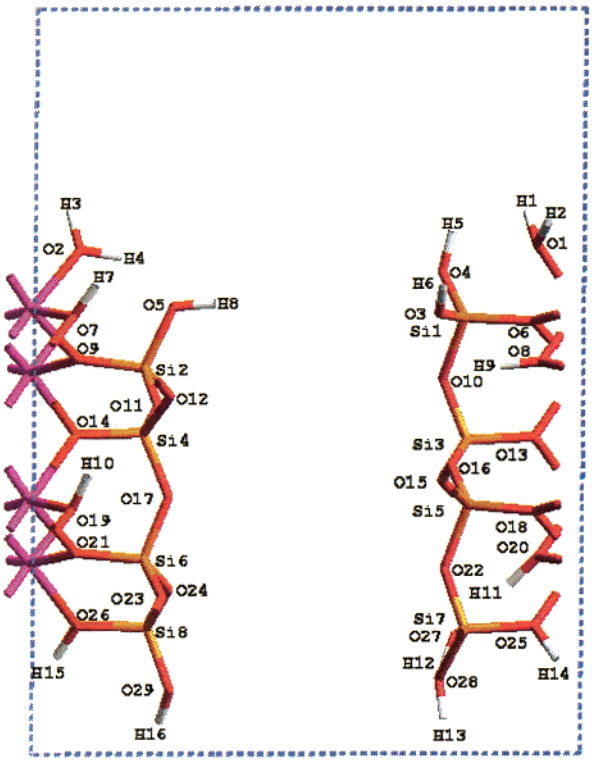

Figure 5. Optimized pyrophyllite lattice-edge unit cell. Three-dimensional periodic boundary conditions are applied at the edges of the cell, as indicated by the blue dashed lines. The color scheme is the same as that used in Figure 2. The atoms are labeled according to their element type and number.

in the models from which they were constructed, we find that they are in general slightly longer. In particular the bond length of the hydroxyl group located in the tetrahedral layer of the Otay-type 1 montmorillonite unit cell, which was 0.9799 Å in the original model, increases to 1.0053 Å in the lattice-edge case. The bond lengths of the hydroxyl groups in the pyrophyllite lattice-edge model are generally slightly longer than their analogues in the Otay-type 1 montmorillonite unit cell. The opposite was true for the original clay models.

Several new hydroxyl groups are created by modeling the broken crystal lattice. These can be grouped according to the atom type(s) to which they are bonded. Six hydroxyl groups in the lattice-edge models are bonded to silicon atoms. Two of the six hydroxyl groups (O5−H8 and O29−H16) reside singly, while the remaining four (O3−H6, O4−H5, O27−H12, and O28−H13) exist as pairs bonded to the same silicon atom. Where two hydroxyl groups are attached to the same silicon atom, one tends to hydrogen bond to the other leading to increased average bond lengths compared to the case where just one hydroxyl group is resident. In general, though, the bond length of the hydroxyl groups bonded to silicon is comparable to those of the octahedral hydroxyl groups. This is not the case for the two hydroxyl groups that bridge octahedral aluminum and tetrahedral silicon atoms (O25−H14 and O26−H16.) These show much longer bond lengths compared to the aforementioned, indicating greater Brønsted acidity. This is attributed to the fact that these hydroxyl groups are bonded to a partially electron-deficient metal atom. The same reasoning accounts for the fact that the two water molecules, which are bonded directly to an octahedral aluminum atom, show even longer hydroxyl bond lengths. Both water molecules show one long hydroxyl bond length (O1−H1 and O2−H4) and one slightly shorter one

(O1−H2 and O2−H3), the longer being the one involved in hydrogen bonding.

6.3.3. Substitution Effects. The Otay-type and Wyoming-type montmorillonite models used in the present work contained an unusually high degree of isomorphic substitution, a direct consequence of the size of our model systems, which was itself constrained by the computational resources available. The degree of substitution affects the charge density of the clay layers and consequently the Brønsted acidity of both the tetrahedral and octahedral hydroxyl groups.

To investigate the extent to which the high charge density affected the Brønsted acidity of the hydroxyl groups several new models were constructed from the original optimized Otay-type 1 montmorillonite unit cell. The new models still exhibited just one substitution of aluminum by magnesium in the octahedral layer and one hydroxyl group in the tetrahedral layer, but one or more of their unit cell length parameters were increased to an integer multiple of its original value. The position of the hydroxyl group in the tetrahedral layer, relative to the magnesium-for-aluminum substitution in the octahedral, remained the same. These new models were optimized with all cell parameters and central octahedral metal ions fixed.

Table 8 (see Appendix A) lists the hydroxyl bond lengths for the various optimized models. The layer charge density has only a small effect on the bond length of the hydroxyl group in the tetrahedral layer with an observed variation of only one-hundredth of an angstrom. No clear relationship between layer charge density and bond length of the hydroxyl group in the tetrahedral layer is observed. Hidden by the average value is the fact that a slight increase of a few-thousandths of an angstrom is observed in the bond length of the octahedral hydroxyl groups with distance from the isomorphic substitution. These results suggest that the net negative charge on the silicate layers is localized around the site of isomorphic substitution and explains why little variation in hydroxyl bond length was observed within the smaller models, where the periodic nature of the unit cells means that the distances between the isomorphic substitution and the hydroxyl groups is always relatively small.

It is postulated from these observations that placement of the hydroxyl group in the tetrahedral layer further away from the site of isomorphic substitution would render it more Brønsted acidic. Therefore two model systems were created from the original optimized Otay-type 1 montmorillonite model, with unit cell parameters $a \times 4b \times c$, as listed in Table 8. These were optimized with all cell parameters and central octahedral metal ions fixed and the hydroxyl group in the tetrahedral layer located at positions a distance of b and $2b$ from the substitution, labeled (2) and (3), respectively, in Figure 6. The location of the hydroxyl group in the original model is labeled (1).

Table 6 lists the hydroxyl bond lengths and total energies of the optimized models. The displacement of the hydroxyl group in the tetrahedral layer from the substitution in the octahedral layer has only a small effect on their bond length, even at the longer distances. In agreement with the pattern indicated by the smaller models, the bond length of the hydroxyl groups in the octahedral layer increases with proximity to the magnesium substitution in the octahedral layer, while that of the hydroxyl groups in the tetrahedral layer decreases. However, again, only a small variation of approximately one-thousandth of an angstrom is observed, which suggests that the hydroxyl groups have similar Brønsted acidity. More interesting is the total energy of the systems which indicates that it is preferable for the hydroxyl group in the tetrahedral layer to exist close to the site of substitution in the octahedral layer, justifying to a certain extent our use of the smaller clay mineral models where this was the case.

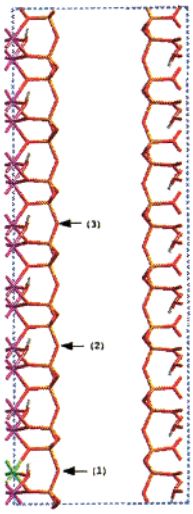

Figure 6. Large Otay-type 1 montmorillonite model. Three-dimensional periodic boundary conditions are applied at the edges of the cell, as indicated by the blue dashed lines. The color scheme is the same as that used in Figure 2. The labels indicate the position of the proton counterion in the optimized models.

Table 6. O−H Bond Lengths and Total Energies of Optimized Otay-Type 1 Montmorillonite Models of Size $a \times 4b \times c$, with the Hydroxyl Group Located at Various Distances from Magnesium-for-Aluminum Substitution in the Octahedral Layer

location of hydroxyl group[a]/Å	Si−(**O**−**H**)−Si/Å	total energy/eV
(1)	0.9802	−47943.5380642
(2)	0.9795	−47942.1412282
(3)	0.9793	−47941.5742591

[a] Refer to Figure 6.

In a similar manner, larger lattice-edge models were constructed to examine the effect of the layer charge density. The average bond length of the various hydroxyl types (octahedral, tetrahedral, those bonded to silicon, those that bridge octahedral aluminum and tetrahedral silicon atoms, and those of the terminating water) are listed in Table 9, Appendix A, for the various optimized models.

As in the case of the nonlattice-edge models, little variation is seen in the bond length of the octahedral hydroxyl groups, of the order of a few ten-thousandths of an angstrom, with a general trend for those furthest from the substitution to be slightly longer. The hydroxyl group located in the tetrahedral layer experiences the biggest variation in bond length.

6.4. Brønsted Acidity of Octahedral Hydroxyl Groups. The octahedral hydroxyl groups hide behind a hexagonal ring-structure formed by the bases of six corner-sharing silicon tetrahedra.[12] The Brønsted acidity of the octahedral hydroxyl groups is therefore only of importance if they are accessible to the monomers. Figure 7 shows the increase in the total energy as a methanal molecule moves through the hexagonal cavity of the Otay-type 3 montmorillonite, toward the octahedral hydroxyl group—the methanal molecule passes through the center of the hexagonal cavity with its carbonyl bond perpendicular to the plane of the interlayer surface. The energy values were calculated by optimization of the system with the methanal molecule at various distances from the *ab* plane. The methanal molecule, the central octahedral metal ions, and all unit cell parameters were fixed during optimization. Optimization of the

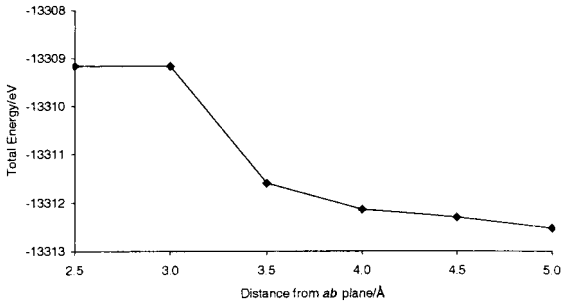

Figure 7. Increase in the total energy of a system when a methanal molecule moves through a hexagonal cavity of an Otay-type montmorillonite.

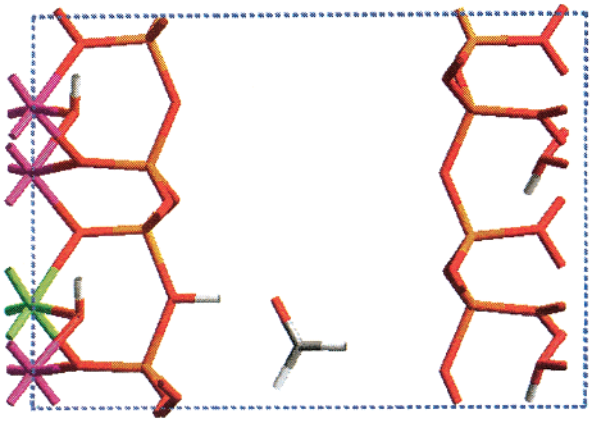

Figure 8. Interaction of methanal with the hydroxyl group located in the tetrahedral layer of Otay-type 1 montmorillonite. Three-dimensional periodic boundary conditions are applied at the edges of the cell, as indicated by the blue dashed lines. The color scheme is the same as that used in Figure 2.

same model systems with the methanal molecule allowed to move showed that the monomer preferred to reside outside the hexagonal ring-structure, within the interlayer. The same was presumed to be true for ethylenediamine since it is a bulkier molecule.

It is possible that a smaller molecule, such as water, may enter through the hexagonal cavity and be protonated by the octahedral hydroxyl. The protonated species could then return to the interlayer and transfer its proton to either monomer. We did not investigate this in the present paper, however.

6.5. Brønsted Acidity of the Hydroxyl Group in the Tetrahedral Layer. Model systems were optimized to examine the interaction of each monomer with the hydroxyl groups in the tetrahedral layer of each of the montmorillonite systems. The bond lengths of these hydroxyl groups are listed in Table 4 and as stated earlier these give an indication of Brønsted acidity. Since the values are all very similar one would expect them to have similar Brønsted acidity and this was found to be true. Protonation of methanal from the hydroxyl groups was not observed in any of the montmorillonite systems, as illustrated in Figure 8. Ethylenediamine, on the other hand, was seen to be protonated in every case. This illustrates the obvious point that the potential of a monomer to be protonated by the clay mineral is as much dependent on its own basicity as the acidity of the hydroxyl group.

Interestingly protonation of methanal was observed when interacting with the hydroxyl group in the tetrahedral layer of the Otay-type 1 montmorillonite model described earlier in Section 6.3.3, where the hydroxyl group was located a distance 2*b* from the site of isomorphic substitution in the octahedral layer. Protonation of methanal was not observed in the analogous model where the hydroxyl group was located only a distance *b* away. This contradicts the tentative pattern suggested by the smaller models, namely that hydroxyl groups in the tetrahedral layer are more Brønsted acidic the further they are from the isomorphic substitution in the octahedral layer. It is thought, however, that the results from the larger models are much more reliable, with the relevant distances in the smaller models being too short to make dependable correlations.

We have already noted that it is more favorable for the proton counterion to reside close to the magnesium-for-aluminum substitution in the octahedral layer, where it is least Brønsted acidic. The weak Brønsted acidity of the hydroxyl groups in the tetrahedral layer is in agreement with experimental work reported in the literature.[20] The implication is that our proposed copolymerization mechanism laid out in Figure 1 is unlikely to be initiated within the clay interlayer.

6.6. Brønsted Acidity of Hydroxyl Groups at the Lattice-Edge. Excluding the octahedral hydroxyl groups that are shown to be sterically inaccessible in Section 6.5, four types of hydroxyl groups are identifiable in the pyrophyllite and montmorillonite lattice-edge structures: those attached to a silicon atom, those bridging a silicon and an aluminum atom, those of the terminating water molecules, and those located in the tetrahedral layer. The bond lengths of these hydroxyl groups are listed in Table 7 and are comparatively much larger than those of the hydroxyl groups located in the tetrahedral layer listed in Table 4. This suggests that they would therefore be more Brønsted acidic. This is indeed the case. Protonation of *both* monomers is facile for all hydroxyl groups present at the lattice-edges, except those bonded to silicon atoms. For hydroxyl groups of this type, protonation of methanal is concurrent with the acceptance of a proton from one of the nearby terminating water molecules. This suggests that catalysis of the polymerization reaction is likely to take place at the lattice-edge, in agreement with Grim's conjecture.[23]

6.7. Lewis Acid Catalysis at the Lattice-Edge. A lattice-edge model was created with an exposed three-coordinate-aluminum in the tetrahedral layer, to act as a possible Lewis acid site. Methanal was observed to coordinate to the aluminum atom via the carbonyl oxygen, forming an aluminum−oxygen bond of length 1.7440 Å. Interestingly this process was concurrent with its protonation by one of the nearby water molecules coordinated to octahedral aluminum, as illustrated in Figure 9. This resulted in a very activated methanal molecule with a carbonyl bond length of 1.4492 Å compared to an in vacuo value of 1.2090 Å. Ethylenediamine was then able to perform nucleophilic attack upon the coordinated methanal. This led to the formation of a hemiaminal and was concurrent with the return of the proton on the methanal to reform a water molecule, as depicted in Figure 10. This caused a slight increase in the length of the aluminum−oxygen bond to 1.7670 Å and a decrease in that of the former carbonyl bond to 1.3724 Å. The newly formed carbon−nitrogen bond was of length 1.5320 Å. Of course, the simultaneous coordination of methanal to the aluminum atom and concomitant protonation is probably an artifact of the way the lattice-edge was modeled and thus somewhat fortuitous. However, these results again confirm the importance of lattice-edges in catalysis by clay minerals.

7. Conclusions

Plane-wave density functional theory based calculations have been performed to optimize periodic models of the clay mineral sodium montmorillonite and to investigate the potential of the

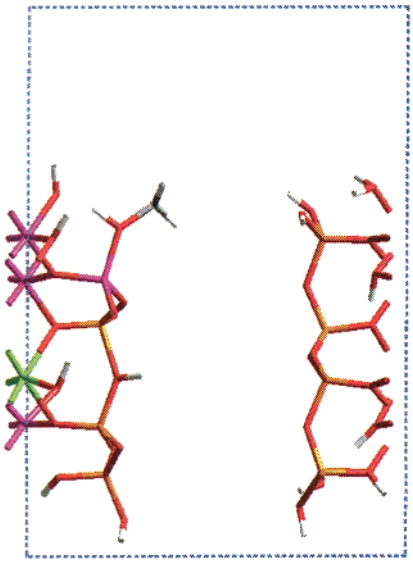

Figure 9. Interaction of methanal with tetrahedral aluminum at the lattice-edge of Otay-type 1 montmorillonite. Three-dimensional periodic boundary conditions are applied at the edges of the cell, as indicated by the blue dashed lines. The color scheme is the same as that used in Figure 2.

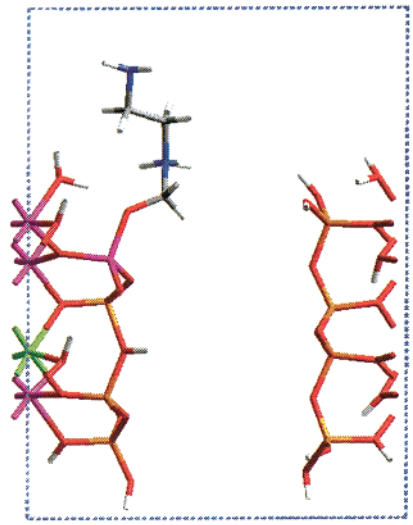

Figure 10. Reaction of ethylenediamine with methanal coordinated to tetrahedral aluminum at the lattice-edge of Otay-type 1 montmorillonite. Three-dimensional periodic boundary conditions are applied at the edges of the cell, as indicated by the blue dashed lines. The color scheme is the same as that used in Figure 2.

acid sites in the models for catalyzing polymerization of methanal with ethylenediamine. The optimized models showed that at low levels, the degree of isomorphic substitution exhibited by the silicate layers has an insignificant effect on the effective Brønsted acidity of hydroxyl groups. However, proximity to sites of isomorphic substitution has a marked effect, with hydroxyl groups located in the tetrahedral layer being more Brønsted acidic when situated further from sites of magnesium-for-aluminum substitution, although it is energetically more favorable for them to be located closer to such sites. Catalysis has been shown to occur at the clay mineral lattice-edge where hydroxyl groups and exposed Al^{3+} ions act as strong Brønsted and Lewis acid sites, respectively.

Table 7. O−H Bond Lengths of Optimized Clay Mineral Lattice-edge Models (Å)

bond[a]	pyrophyllite	Otay-type 1 montmorillonite
O1−H1	1.0036	1.0240
O1−H2	0.9999	0.9796
O2−H3	0.9905	0.9843
O4−H4	0.9959	1.0063
O3−H6	0.9799	0.9729
O4−H5	0.9813	0.9763
O5−H8	0.9727	0.9795
O7−H7	0.9724	0.9745
O8−H9	0.9745	0.9707
O17−H17	-	1.0053
O19−H10	0.9705	0.9727
O20−H11	0.9804	0.9758
O25−H14	0.9974	0.9890
O26−H15	0.9945	0.9895
O27−H12	0.9769	0.9741
O28−H13	0.9790	0.9777
O29−H16	0.9718	0.9727

[a] O−H bond labels refer to Figure 5.

Table 8. Average O−H Bond Lengths of Hydroxyl Groups Located in the Octahedral and Tetrahedral Layers of Optimized Otay-type 1 Montmorillonite Models of Various Size (Å)

cell size[a]	*Al*−(**O**−**H**)−*Al*	*Si*−(**O**−**H**)−*Si*
$a \times b \times c$	0.9707	0.9799
$2a \times b \times c$	0.9704	0.9807
$2a \times 2b \times c$	0.9707	0.9811
$a \times 4b \times c$	0.9712	0.9802

[a] $a = 5.18$ Å, $b = 9.02$ Å, $c = 13.24$ Å.

Table 9. Average O−H Bond Lengths of the Hydroxyl Group Types Present in Optimized Otay-Type 1 Montmorillonite Lattice-Edge Models of Various Size (Å)

cell size[a]	Al−(**O**−**H**)−Al	Si−(**O**−**H**)−Si	Si−**O**−**H**	Al−(**O**−**H**)−Si	Al−(**O**−**H**)−H
$a \times b \times c$	0.9734	1.0053	0.9755	0.9893	0.9985
$2a \times b \times c$	0.9737	0.9909	0.9766	0.9981	0.9978
$a \times 2b \times c$	0.9729	0.9917	0.9765	0.9977	0.9973

[a] $a = 5.18$ Å, $b = 17.50$ Å, $c = 13.24$ Å.

Appendix A: Hydroxyl Bond Lengths of Optimized Montmorillonite Structures

Tables 7−9 containing O−H bond lengths.

Acknowledgment. We are very grateful to Professor M. C. Payne, Dr. M. I. J. Probert, Dr. M. D. Segall, and Dr. P. J. Hasnip for useful advice and comments on the CASTEP code and Dr. A. Whiting for stimulating discussions on possible catalytic mechanisms. We thank HEFCE (U.K.) for funding the purchase of our Silicon Graphics Onyx2 machine under the JREI scheme and Professor M. C. Payne and Cambridge University High Performance Computing Facility for use of their Origin2000 machine. We acknowledge Dr. S. P. Newman for his comments on the manuscript. The Ph.D. studentship of S. Stackhouse is funded by Queen Mary, University of London, and W.R. Grace & Co.

JA015808D